Quantum Mechanical and Rice−Ramsperger−Kassel−Marcus Investigation of the Thermal Unimolecular Decomposition of CF_2BrO and CF_2ClO Radicals

Evangelos Drougas,[†] Agnie M. Kosmas,*[,†] and Abraham F. Jalbout[‡]

Department of Chemistry, University of Ioannina, Greece 451 10, and Department of Chemistry, Division of Materials Science, The University of Arizona, Tucson, Arizona 85712

Received: February 5, 2004

Quantum mechanical and Rice−Ramsperger−Kassel−Marcus calculations are carried out to study the thermal unimolecular decomposition of CF_2XO radicals (X = Br, Cl). Two kinds of dissociation mechanisms are possible, carbon−halogen bond scission and intramolecular three-center XF elimination. It should be noted that the three-center direct XF elimination has only been able to be characterized at the B3LYP level. X-atom elimination is shown to be the dominant reaction pathway, whereas C−F bond scission and XF elimination have been found to exhibit high energy barriers. On the basis of the ab initio data, energy-specific rate constants $k(E)$ and thermal rate constants $k(T,P)$ are evaluated using master equation numerical analysis.

Introduction

Formation of haloalkoxy radicals has been repeatedly confirmed in studies of the photolytic oxidation of haloalkanes.[1−13] Because of the capacity of many such radicals to release active bromine and chlorine atoms in the stratosphere, many experimental and theoretical studies have been devoted to their chemical activity including various unimolecular decomposition pathways and reactions with molecular oxygen and nitrogen monoxide.[14−29]

The brominated and chlorinated fluoromethoxy radicals in particular[4−5,11,15] have been shown in all experimental studies investigating their atmospheric fate to decompose by releasing Cl and Br atoms

$$CF_2BrO \rightarrow CF_2O + Br$$

$$CF_2ClO \rightarrow CF_2O + Cl$$

They thus show interesting peculiarities compared to corresponding hydrogenated species. For instance, CH_2ClO, in several studies of the unimolecular dissociation pathways, has shown no evidence for loss of Cl atoms,[18] which is consistent with the rather significant barrier of the order of 11 kcal mol^{-1} [24] calculated for the C−Cl bond scission. Instead, elimination of HCl has been found to be the preferred decomposition pathway.[24,28] However, it has been suggested that the breaking of the C−Cl bond may be facilitated by the presence of another halogen atom such as fluorine[16] or chlorine.[28] Indeed, F_2CClO[16] and Cl_2CHO[28] are shown to eliminate a chlorine atom easily rather than suffer the three-center molecular elimination. Br-atom elimination, on the other hand, has always been found to be the preferred decomposition pathway.[10,17,25−26] C−Br bond breaking in CH_2BrO presents a much lower energy barrier of only 2.6 kcal mol^{-1}, while HBr elimination exhibits a higher barrier, 11.5 kcal mol^{-1}.[26] Thus, the chloromethoxy and bromomethoxy radicals present varying patterns of unimolecular decomposition, and it would be interesting to examine and compare with the dissociation pathways of the corresponding brominated and chlorinated fluorine containing species. In contrast to C−Cl and C−Br bond scissions, the C−F bond is particularly strong and F atom elimination has not been observed.[16, 29]

No theoretical studies exist for the thermal decomposition of CF_2BrO. For CF_2ClO, the modified neglect of diatomic overlap (MNDO) calculations of Rayez et al.[14] have shown that the C−Cl bond is quite weak. Li and Francisco,[16] performing ab initio molecular orbital and Rice−Ramsperger−Kassel−Marcus (RRKM) calculations in the investigation of Cl and F elimination pathways from $CCl_{3-x}F_xO$ radicals, have shown that Cl elimination is the probable decomposition pathway while the breaking of the C−F bond is very unlikely. In the present work, we employ quantum mechanical and RRKM methods to study the decomposition pathways of CF_2XO radicals, X = Br, Cl, and more specifically: (i) the most important stationary points on the potential energy surface, (ii) the overall reaction mechanism including bond scission and three-center elimination, (iii) the energy-specific rate constants of various reaction channels, and (iv) the macroscopically observable rate constants for X elimination from CF_2XO and the falloff behavior.

Computational Details

The following reaction channels were considered in the calculations

$$CF_2XO \rightarrow CF_2O + X \qquad X = Cl, Br \qquad (1)$$

$$\rightarrow CFXO + F \qquad (2)$$

$$\rightarrow CFO + XF \qquad (3)$$

Reactions 1 and 2 are characterized as β-bond scission channels, i.e., decompositions where a bond is broken on a site adjacent to the radical site. Reaction 3 represents the three-center XF molecular elimination.

A. Quantum Mechanical Calculations. The geometries of reactants, products, and transition states were optimized at the B3LYP/6-311G(d,p) and UMP2(full)/6-311G(d,p) levels of

* To whom correspondence may be addressed. E-mail: amylona@cc.uoi.gr.
[†] University of Ioannina.
[‡] The University of Arizona.

10.1021/jp040104m CCC: $27.50
Published on Web 06/17/2004

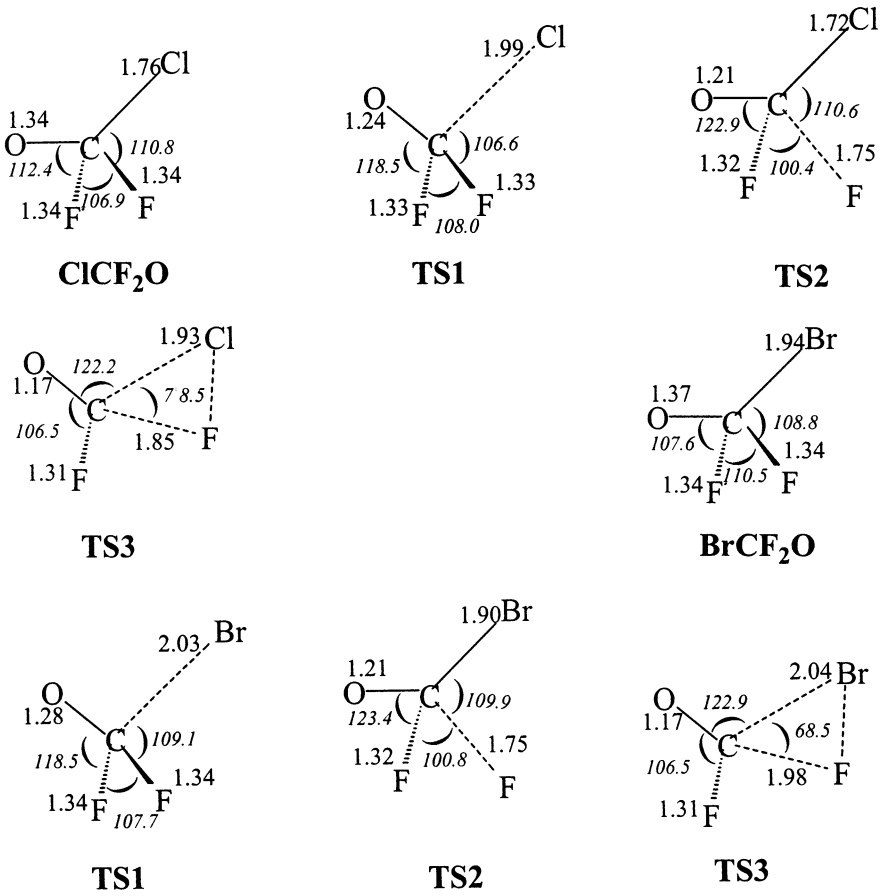

Figure 1. Minimum-energy and transition-state geometries for $CBrF_2O$, $CClF_2O$ decomposition pathways. Structural parameters for TS1, TS2 at the UMP2(full)/6-311G(d,p) level and for TS3 at the B3LYP/6-311G(d,p) level.

TABLE 1: Moments of Inertia (I_A, I_B, I_C) and Harmonic Vibrational Frequencies for Minima and Transition States of XCF_2O Decomposition at the UMP2/6-311G(d,p) Level

	I_A, I_B, I_C/amu	frequencies/cm^{-1}
$CBrF_2O$	307, 847, 868	306, 336, 346, 520, 742, 744, 1080, 1245, 1261
TS1	304, 840, 851	384i, 251, 337, 373, 556, 559, 884, 1257, 1377
TS2	318, 847, 919	1224i, 210, 308, 373, 398, 595, 734, 1171, 1662
TS3	365, 787, 844	200i, 175, 221, 325, 341, 540, 678, 1122, 2048
$CClF_2O$	309, 525, 532	308, 311, 459, 541, 562, 774, 1019, 1240, 1295
TS1	296, 555, 571	978i, 256, 331, 455, 574, 582, 927, 1297, 1481
TS2	313, 530, 599	1207i, 231, 336, 447, 506, 583, 787, 1202, 1669
TS3	342, 540, 572	700i, 220, 260, 369, 390, 520, 668, 1119, 2058

theory, and consistent results have been obtained by both methods. The larger basis set was preferred for the optimization procedure rather than the standard 6-31G(d) basis set, usually employed in the original G2MP2 scheme which has been subsequently used for the energy calculations as we shall see next. Harmonic frequencies have been calculated at the same levels to characterize the stationary points, and transition states were identified by one imaginary frequency as first-order saddle points. Intrinsic reaction coordinate calculations have been performed to confirm that each transition state is linked to the desired reactants and products. Three transition state structures, denoted as TS1, TS2, and TS3, have been determined for each system and for reactions 1, 2, and 3, respectively. TS3 has only been determined at the B3LYP/6-311G(d,p) level as it will be described in detail below. The geometrical parameters are given in Figure 1, and Table 1 summarizes the harmonic vibrational frequencies and the moments of inertia.

To refine the energetics, two series of higher-level calculations have been performed. In the first, the energetics of the system has been examined by single-point coupled-cluster, CCSD(T)/6-311G(d,p), calculations at the UMP2(full)/6-311(d,p)-optimized geometries. In the second series, the inexpensive and widely used G2MP2[30] method has been employed, which is a modified version of G2[31] using MP2 instead of MP4 for the basis-set extension corrections. G2MP2 has been used in the theoretical investigation of several haloalkoxy radicals,[24−28] and thus, it provides a common ground for comparison. Table 2 summarizes the total electronic energies and energy differences determined at various levels of theory, and the reaction energy profiles based on the CCSD(T) and G2MP2 computations are depicted in Figures 2 and 3. Overall, the G2MP2 results are found to be in the same direction with the higher-accuracy, full-electron correlation CCSD(T) calculations, but they do show a tendency to overestimate the barriers compared to the latter method.

The calculations have been carried out using the Gaussian 98 series of programs.[32]

As mentioned above, the transition-state configuration for XF elimination has not been able to be determined at the MP2 level. All attempts to locate this transition state proved futile since stretching the C−F and C−X bonds and reducing the FCX bond angle invariably led to TS1 or TS2. Only the tedious effort at the B3LYP/6-311G(d,p) level of theory has succeded to produce this transition-state geometry. The configuration obtained is consistent with the corresponding structure calculated for the HF elimination in the CHF_2O radical,[29] and thus, this geometry has been considered reasonable, and it was adopted for the energy calculations. Problems in the determination of the transition-state geometry for the three-center molecular eliminations have also been encountered by other workers. For instance, in the study of CH_2ClO and $CHCl_2O$ decompositions by Wang

TABLE 2: Total Electronic Energies (Hartrees) and Energy Difeerences (kcal mol^{-1}) for the Unimolecular Decomposition of CXF_2O Radicals Including ZPE Corrections (kcal mol^{-1})

	UMP2/6-311G(d,p)[a]	ΔE	CCSD(T)//UMP2/6-311G(d,p)	ΔE	G2MP2	ΔE[b]	ZPE
CF_2BrO	−2884.82317	0.0	−2884.86291	0.0	−2885.16825	0.0	8.7
TS1	−2884.82070	0.5	−2884.86092	0.2	−2885.16630	1.2	7.7
TS2	−2884.75902	38.1	−2884.81757	30.3	−2885.11494	33.5	6.8
TS3	−2884.73677	53.2	−2884.82807	20.9	−2885.10734	38.2	7.7
CF_2O+Br	−2884.88124	-36.6	−2884.90514	-26.5	−2885.20520	-23.2	8.8
CFBrO+F	−2884.79689	16.5	−2884.82054	25.2	−2885.12623	26.4	7.3
CFO+FBr	−2884.76495	34.0	−2884.82989	18.2	−2885.11089	36.0	6.2
CF_2ClO	−771.97378	0.0	−772.02270	0.0	−772.32782	0.0	9.1
TS1	−771.96143	6.3	−772.01645	2.5	−772.31789	6.2	7.7
						11.9[6]	
						10.5[4]	
						12.4[14]	
						2.4[16]	
TS2	−771.91259	36.5	−771.97220	29.8	−772.28034	29.8	7.2
						28.2[14]	
TS3	−771.89350	48.8	−771.96694	33.4	−772.26533	39.2	7.5
CF_2O + Cl	−772.01360	−24.7	−772.04217	-11.9	−772.34861	-13.0	8.8
CFClO + F	−771.94898	14.1	−771.98432	22.7	−772.29091	23.2	7.7
CFO + FCl	−771.90036	43.3	−771.97020	30. 1	−772.26807	37.5	6.3

[a] The values given in the G2MP2 output. [b] The supescripts in the ΔE column indicate the appropriate references.

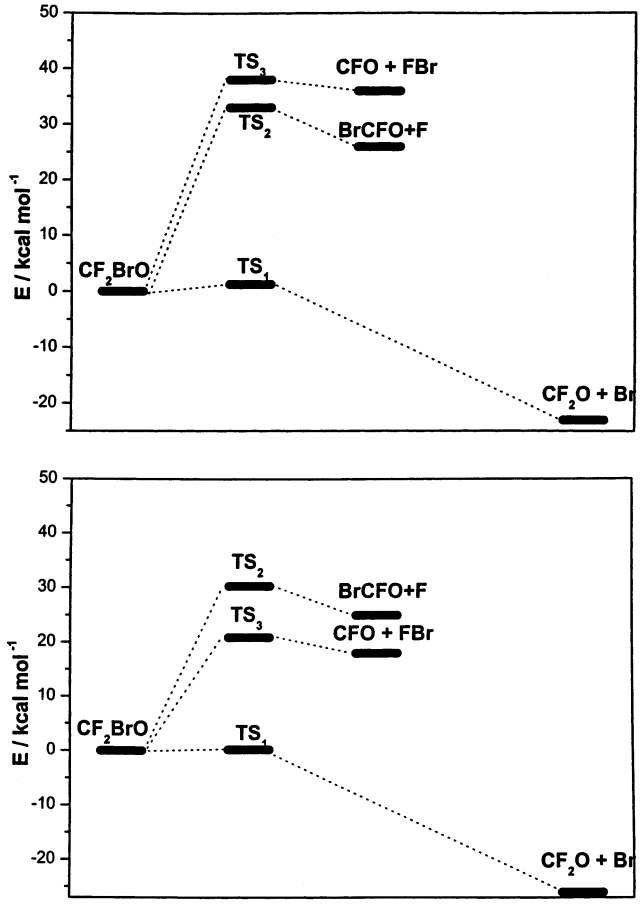

Figure 2. Important stationary points on the potential-energy surface for $CBrF_2O$ decomposition at the G2MP2 level (top) and CCSD(T) level (bottom).

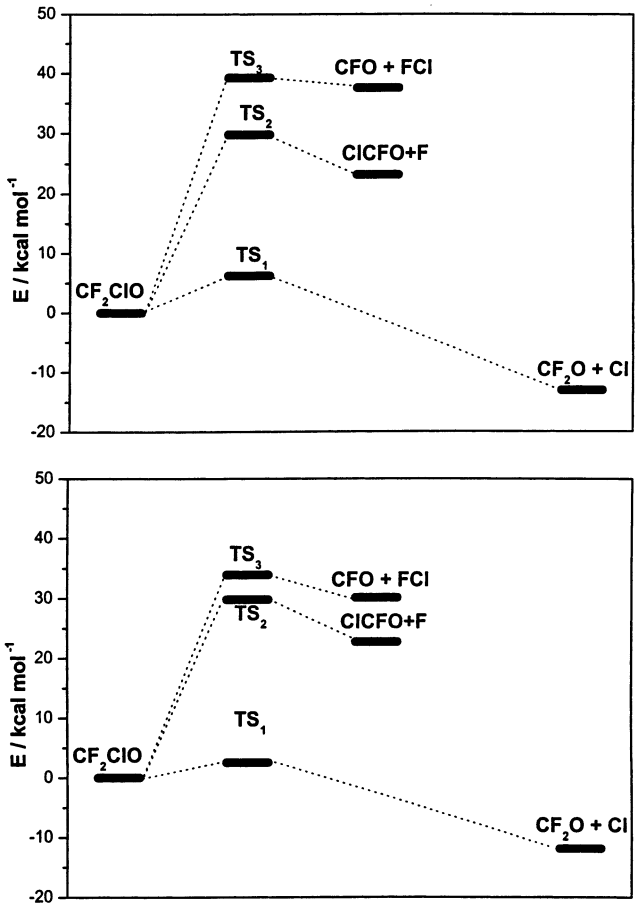

Figure 3. Important stationary points on the potential-energy surface for $CClF_2O$ decomposition at the G2MP2 level (top) and CCSD(T) level (bottom).

et al.[27] and Hou et al.,[28] the transition-state geometries for HCl elimination have been very difficult to be determined. Indeed, for the former system, solution of this problem has been established much later,[28] while for the latter, this determination has been achieved only at the semiempirical AM1 level.[28] Wu and Carr[24] have also encountered problems at the MP2/6-31G(d) level in the location of the HCl elimination transition state for the CH_2ClO system. The transition-state geometry has been determined only at the higher MP2/6-31(d,p) level. As we shall see in the next section, uncertainty regarding the FCl, FBr molecular and the Cl, Br atomic elimination channels also arises with respect to the energy results since the G2MP2 and the single-point CCSD(T) calculations produce different energy barriers. Thus, it is reasonable to assume that the difficulties in the location of the XF elimination transition states probably originate from the low strength values of C−Cl and C−Br bonds, which easily direct the decomposition to the atomic elimination channels.

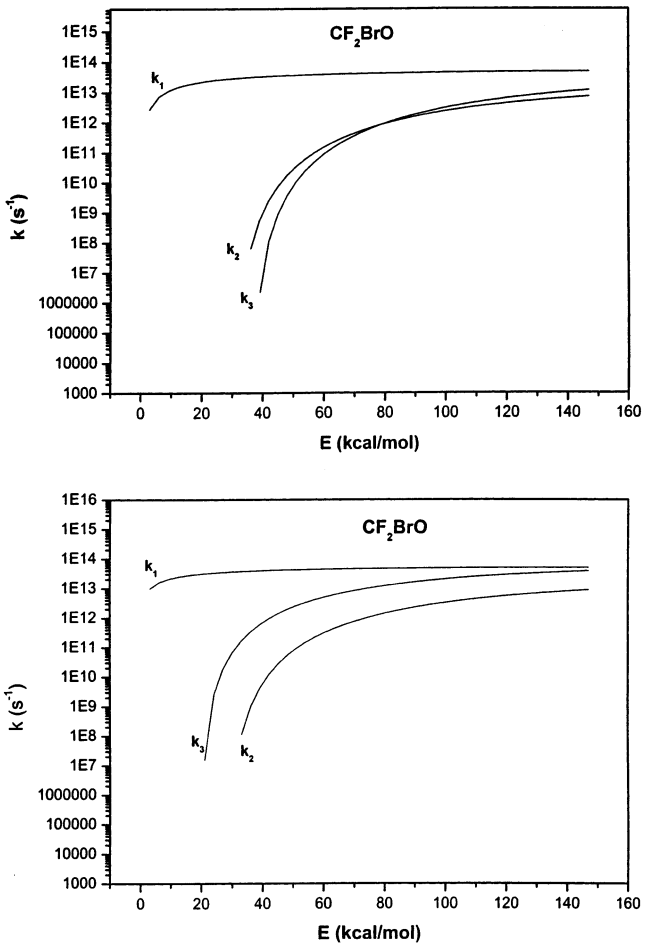

Figure 4. Energy-specific unimolecular rate constants for $CBrF_2O$ decomposition based on the G2MP2 level (top) and CCSD(T) level (bottom).

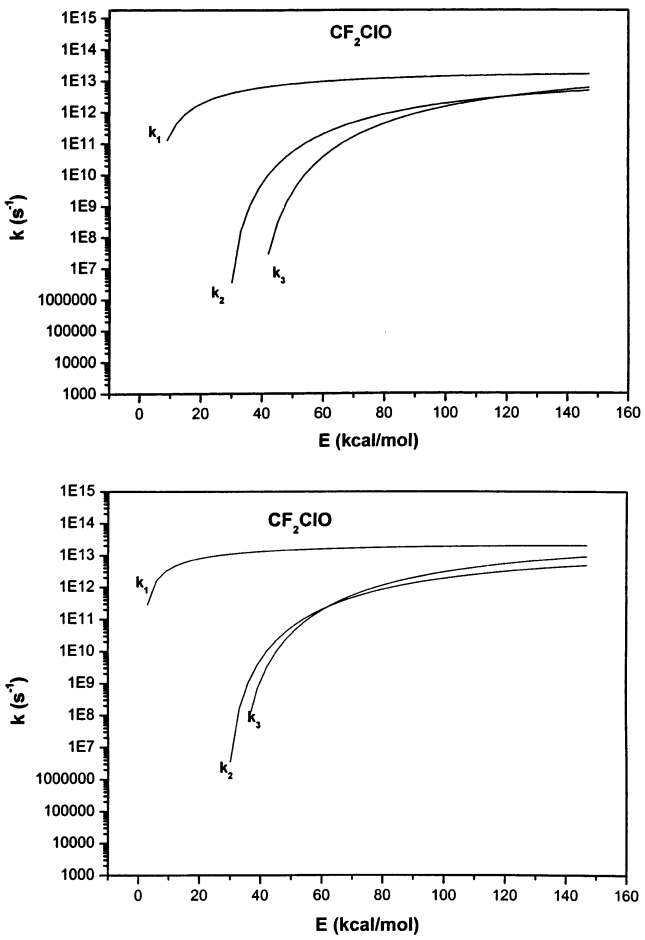

Figure 5. Energy-specific unimolecular rate constants for $CClF_2O$ decomposition based on the G2MP2 level (top) and CCSD(T) level (bottom).

B. Kinetic Calculations. On the basis of the ab initio data, energy-specific rate constants, $k(E)$, for the various unimolecular pathways are evaluated using RRKM theory[33−36]

$$k(E) = \int_0^{E-E_0} \rho_{TSi}(E_+)\, dE_+ / h\rho_M(E) \qquad (4)$$

where $\rho_{TSi}(E_+)$ is the density of states for the active degrees of freedom of the transition state TSi involved in the reaction step i and $\sigma_M(E)$ is the density of states available to the reactant minimum M at an energy E.

Thermal rate constants and falloff curves are computed at various temperatures and pressures through the numerical solution[35] of the master equation[37] which gives the unimolecular rate coefficient, k_{uni}, at any temperature and pressure

$$-k_{uni}g(E) = \omega \int_0^{\infty} (P(E,E')g(E') - P(E',E)g(E))\, dE' - k(E)g(E) \qquad (5)$$

$k(E)$ is the microscopic reaction rate coefficient, $g(E)$ denotes the population of molecules with energy E, $P(E,E')$ is the probability of energy tranferred per collision, and ω is the collision frequency. The resulting $k(T)$ Arrhenius expressions and the $k(T,P)$ falloff curves are given in Figures 6 and 7.

The kinetic calculations were performed numerically by employing the UNIMOL[38] suite of programs, consisting of two separate main algorithms. The first, called RRKM, carries out microcanonical rate coefficient calculations and computes high-pressure limit rate parameters. It also generates a file containing all data which will be subsequently used in the solution of the master equation. An energy grain size of 0.05 kcal mol^{-1} has been used. The second program, MASTER, gives a numerical solution of the master equation with an energy transfer $P(E,E')$ functional form described by the biased random walk model. It computes the low-pressure limit rate coefficient, the collisional efficiency (β), and a complete falloff curve around a median pressure. The detailed calculation method and basic theory used are given in detail by Gilbert et al.[35] The Lennard-Jones potential parameters (i.e., well depth ϵ and collision diameter σ) for CF_2XO-N_2 are not available in the literature. Thus, suitably adjusted parameters for the present fluorinated radicals had to be estimated in analogy with the values employed for the corresponding chlorinated and brominated methoxy analogues.[24−26] The estimated data, $\epsilon = 250$ K and $\sigma = 5.2$ Å, have been used in the falloff calculations.

Reaction Mechanism

Processes 1 and 2 correspond to the cleavage of C−X and C−F bonds, respectively, and reaction 3 gives the three-center XF molecular elimination channel. They take place through the transition states TS1, TS2, and TS3. Elimination of the Br or Cl atom presents by far a much lower energy barrier than the C−F bond scission and the XF elimination, and thus, it is found to be the most feasible process in both Br and Cl cases at all levels of calculations.

A. X−β-Bond Scission Mechanism. TS1 configurations result from the simple elongation of the C−Br or the C−Cl

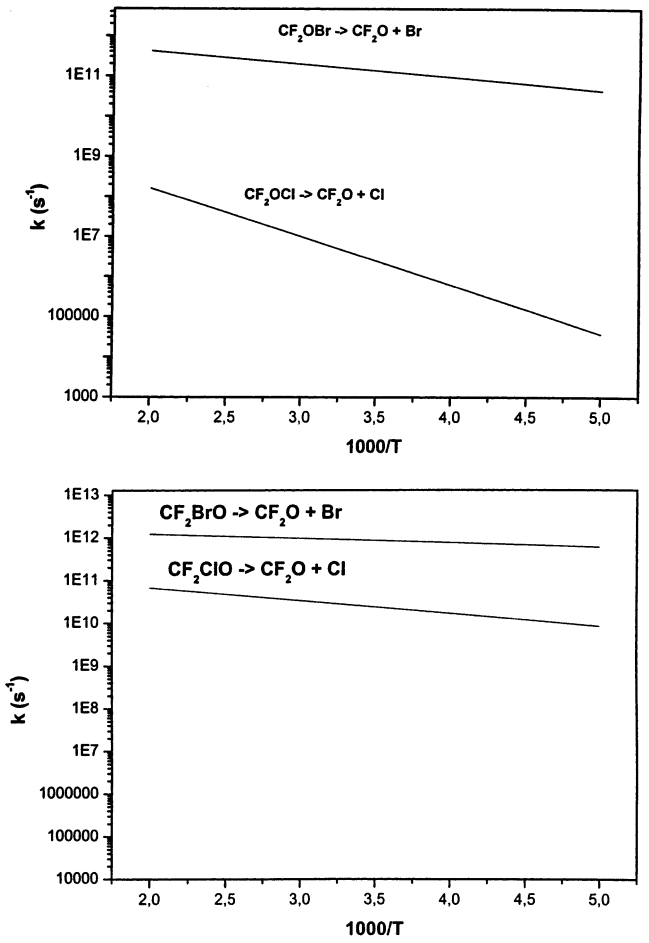

Figure 6. Arrhenius kinetic expressions for Br, Cl atom elimination based on the G2MP2 level (top) and CCSD(T) level (bottom).

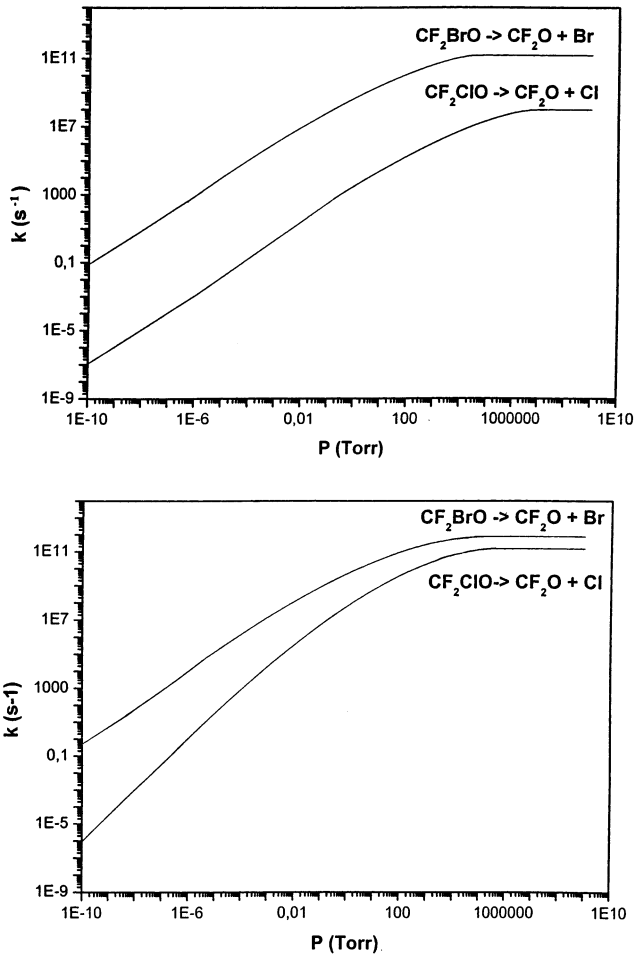

Figure 7. Falloff curves for Br, Cl atom elimination based on the G2MP2 level (top) and CCSD(T) level (bottom).

bonds and the corresponding shrinkage of the C−O bond. They are located at 0.2, 2.5 kcal mol^{-1} at the CCSD(T) level and 1.2, 6.2 kcal mol^{-1} at the G2MP2 level above reactant for X = Br and Cl, respectively. The main conclusion is that the CCSD(T) method produces systematically lower barrier values that are more realistic than the G2MP2 values. We also observe that removal of the Br atom involves an even lower barrier than that of the Cl atom at all levels of calculations. Furthermore, comparison with the calculated barriers for the corresponding hydrogenated species, CH_2BrO[26] and CH_2ClO,[24] indicates that the replacement of hydrogen by fluorine lowers the critical energy for X-atom elimination. It is also interesting to compare the present results with the experimental estimates and the theoretical values reported in the literature for the activation energy of Cl-atom elimination. As we realize from Table 2, there is a wide spread of values for this barrier reported by various workers. The experimental estimates[4,6] and the MNDO results of Rayez et al.[14] predict unreasonably high values for the activation barrier of Cl elimination, in the vicinity of 10 kcal mol^{-1}. The calculations of Li and Francisco[16] produce a much lower value and agree with the present CCSD(T) result. In our opinion, the ease in Cl-atom elimination observed experimentally is consistent with a very low value of the activation barrier. Indeed, such a conclusion is also supported by Wu and Carr,[6] who, in their investigation of CF_2ClO decomposition, argue that the observed temperature dependence of the Cl-atom elimination rate coefficients is significantly less than expected for an activation energy in the vicinity of 10 kcal mol^{-1}. Thus, the present CCSD(T) calculations and the calculations of Li and Francisco, that lead to an activation barrier around 2.5 kcal mol^{-1}, may be considered to be the most reasonable. The G2MP2 barrier on the other hand appears consistent with the experimental lower limit rate estimates. We have thus constructed the reaction energy profiles and performed the kinetic calculations based on both methodologies and a useful comparison is carried out.

B. F−*β*-Bond Scission Mechanism. TS2 geometries are formed in a similar way as TS1 geometries, i.e., by the significant elongation of the C−F bond by about 0.4 Å and the corresponding shrinkage of the C−O bond. However, the associated barriers for such a configuration are considerably larger in both systems, indicating the high strength of the C−F bond compared to the weaker C−Cl and C−Br bonds. The consistency between the calculated results among all methods is remarkable, particularly in the CF_2ClO case where both CCSD(T) and G2MP2 methods produce exactly the same result for the barrier height, 29.8 kcal mol^{-1}, in excellent agreement with the barrier reported by Li and Francisco,[14] 28.2 kcal mol^{-1}.

C. Three-Center Molecular Elimination. Reaction 3 represents the direct three-center elimination of the XF species. The transition-state configuration TS3 results from the significant elongation of both C−F and C−X bonds and the decrease of the XCF bond angle. It is considerably high located with respect to reactant in both the $CClF_2O$ and $CBrF_2O$ radicals. However, large differences are observed between the CCSD-(T) and the G2MP2 methods with the latter producing much higher barriers than the former. In BrF elimination in particular, the CCSD(T) barrier, 20.9 kcal mol^{-1}, is almost half the G2MP2 result, 38.2 kcal mol^{-1}, and inverses the activation barrier order

in $CBrF_2O$ decomposition, predicting that BrF elimination is more feasible thermodynamically than F-atom removal. In the Cl case, the barrier is only lowered by about 6 kcal mol^{-1} compared to the G2MP2 result. The differences probably arise from the lower C−Br and C−Cl bond strength values predicted by the CCSD(T) computations as reflected in the corresponding C−Br and C−Cl bond scission processes. It would be interesting to extend the present CCSD(T) calculations using higher basis sets to further investigate this effect. However, our limited computing resources and the little overall importance of these reaction channels in $CBrF_2O$ and $CClF_2O$ decomposition mechanism have prevented us from doing so.

Rate-Constant Results

Two series of kinetic calculations have been performed, i.e., based on CCSD(T) and G2MP2 results. The resulting $k_i(E)$, depicted in Figures 5 and 6 as a function of the internal energy E, follow the critical energies order with $k_1(E)$ calculated to be much higher than $k_2(E)$ and $k_3(E)$.

Since C−Br and C−Cl bond scissions dominate the decomposition process, unimolecular thermal rate coefficients, $k(P,T)$, were calculated only for the most important decomposition channel (1) leading to X-atom elimination. The quantitative determination requires the exact solution of the master equation.[37] A numerical evaluation has been carried out using the UNIMOL algorithm[38] as described in the previous section. For the interesting temperature range 250−500 K and atmospheric pressure of 760 Torr with N_2 as the bath gas, this calculation has yielded the following Arrhenius equations

$$k_{Br}(T) = 1.9 \times 10^{12} \exp(-751/T)$$

$$k_{Cl}(T) = 4.3 \times 10^{10} \exp(-2792/T)$$

based on the G2MP2 calculations and

$$k_{Br}(T) = 2.1 \times 10^{12} \exp(-313/T)$$

$$k_{Cl}(T) = 5.4 \times 10^{11} \exp(-1041/T)$$

based on the CCSD(T) results. The corresponding rate constant curves presented in Figure 7 reflect the large discrepancies observed in the energetics. The predicted activation energies using the CCSD(T) results are much lower than the ones based on the G2MP2 method producing considerably higher k values. Other differences are encountered in the relative magnitude among the two systems. Thus, the decomposition rate of CF_2BrO, which is more than 3 orders of magnitude higher than that of CF_2ClO at the G2MP2 level over the temperature studied, differs only by 1 order of magnitude at the CCSD(T) level. Both results, however, demonstrate the relative weakness of the C−Br bond compared to the C−Cl bond. The effect is consistent with the reactivity trends observed in the cases of CH_2BrO, CH_2ClO and CH_3CHBrO, CH_3CHClO radicals.[24−28] In the chlorinated derivatives, because of the moderate strength of the C−Cl bond, C−Cl bond scission is less probable, and the HCl elimination prevails over the Cl-atom removal. Br-atom elimination, on the other hand, is always favored in the brominated analogues.

Figure 7 presents the corresponding falloff curves for k_{Br} and k_{Cl} at 298 K. The rates approach the high-pressure limit near 10^3 and 10^5 Torr, respectively, at the G2MP2 level and 10^3 and 10^4 Torr, respectively, at the CCSD(T) level. At 750 Torr and the lower pressures dominating in the stratosphere, the rate constants are well within the falloff regime. It would interesting to compare the theoretical results with the existing lower limit experimental evidence. Wu and Carr[4] have estimated the unimolecular rate constant for the decomposition of CF_2ClO to be $(6.4 \pm 1.4) \times 104$ s^{-1} at 298 K and pressure 4−20 Torr. A direct comparison with the theoretical predictions is given in Table 3, where a quite fair agreement is observed.

TABLE 3: Unimolecular Rate Constant k_{Cl} (s^{-1}) at 298 K for $CClF_2O$ Decomposition

total pressure (Torr)	G2MP2	CCSD(T)	experimental estimate[a]
4	3.7×10^4	7.3×10^6	
7	6.5×10^4	1.0×10^7	$(6.4 \pm 1.4 \times 10^4)$
10	9.3×10^4	1.2×10^8	
13	1.2×10^5	1.4×10^8	
16	1.5×10^5	1.8×10^8	
20	1.9×10^5	3.0×10^8	

[a] The experimental lower limit estimate is from ref 6.

Summary

Carbon−halogen bond scission and intramolecular three-center elimination pathways have been examined in detail for the decomposition mechanism of $CBrF_2O$ and $CClF_2O$ radicals at various levels of quantum electronic molecular theory. The coupled cluster, CCSD(T), results produce considerably lower and more realistic critical energies than the G2MP2 calculations for Br, Cl atom removal.

Kinetic calculations were carried out based on RRKM theory and using a numerical evaluation of the master equation. The calculated Arrhenius expressions and the falloff curves are found in good agreement with the lower limit experimental estimate.

References and Notes

(1) Simonaitis, R.; Glavas, S.; Heicklen, J. *Geophys. Res. Lett*. **1979**, *6*, 385.
(2) Francisco, J. S.; Williams, I. H. *Int. J. Chem. Kinet.* **1988**, *20*, 455.
(3) Atkinson, R. *J. Phys. Chem. Ref. Data* **1989**, Monograph No. 1.
(4) Carr, R. W.; Peterson, D. G.; Smith, F. K. *J. Phys. Chem*. **1986**, *90*, 607.
(5) Lesclaux, R.; Caralp, F.; Dognon, A. M. *Geophys. Res. Lett*. **1986**, *13*, 933.
(6) Wu, F.; Carr, R. W. *J. Phys. Chem.* **1992**, *96*, 1743.
(7) Wallington, T. J.; Hurley, M. D.; Ball, J. C.; Kaiser, E. W. *Environ. Sci. Technol.* **1992**, *26*, 1318.
(8) Catoire, V. A.; Lesclaux, R.; Lightfoot, P. D.; Rayez, M. T. *J. Phys. Chem*. **1994**, *98*, 2889.
(9) Wallington, T. J.; Orlando, J. J.; Tyndall, G. S. *J. Phys. Chem*. **1995**, *99*, 9437.
(10) Orlando, J. J.; Tyndall, G. S.; Wallington, T. J. *J. Phys. Chem*. **1996**, *100*, 7026.
(11) Bilde, M.; Sehested, J.; Mogelberg, T. E.; Wallington, T. J.; Nielsen, O. J. *J. Phys. Chem*. **1996**, *100*, 7050.
(12) Mogelberg, T. E.; Sehested, J.; Wallington, T. J.; Nielsen, O. J. *Int. J. Chem. Kinet*. **1997**, *29*, 209.
(13) Orlando, J. J.; Tyndall, G. S. *J. Phys. Chem. A* **2002**, *106*, 312.
(14) Rayez, J. C.; Rayez, M. T.; Halvick, P.; Duguay, B.; Lesclaux, R.; Dannenberg, J. J. *Chem. Phys.* **1987**, *116*, 203.
(15) Lesclaux, R.; Dognon, A. M.; Caralp, F. *J. Photochem. Photobiol.* **1987**, *41*, 1.
(16) Li, Z.; Francisco, J. S. *J. Am. Chem. Soc.* **1989**, *111*, 5660.
(17) Chen, J.; Catoire, V.; Niki, H. *Chem. Phys. Lett.* **1995**, 245, 519.
(18) Wu, F.; Carr, R. W. *Chem. Phys. Lett*. **1999**, *305*, 44.
(19) Wang, B.; Hou, H.; Gu, Y. *J. Phys. Chem. A* **1999**, *103*, 2060.
(20) Hou, H.; Wang, B.; Gu, Y. *J. Phys. Chem. A* **2000**, *104*, 1570.
(21) Wu, F.; Carr, R. W. *J. Phys. Chem. A* **2001**, *105*, 1423.
(22) Kukui, A.; Le Bras, G. *PhysChemChemPhys* **2001**, *3*, 175.
(23) Somnitz, H.; Zeller, R. *PhysChemChemPhys* **2001**, *3*, 2352.
(24) Wu, F.; Carr, R. W. *J. Phys. Chem. A* **2002**, *106*, 5832.
(25) Drougas, E.; Kosmas, A. M. *Chem. Phys. Lett.* **2003**, *379*, 297.
(26) Drougas, E.; Kosmas, A. M. *Chem. Phys.* **2004**, *300*, 233.
(27) Wang, B.; Hou, H.; Gu, Y. *J. Phys. Chem. A* **1999**, *103*, 2060.
(28) Hou, H.; Wang, B.; Gu, Y. *J. Phys. Chem. A* **1999**, *103*, 8075.

(29) Zachariah, M. R.; Tsang, W.; Westmoreland, P. R.; Burgess, D. R. F., Jr. *J. Phys. Chem*. **1995**, *99*, 12512.

(30) Curtiss, L. A.; Raghavachari, K.; Pople, J. A. *J. Chem. Phys.* **1993**, *98*, 1293.

(31) Curtiss, L. A.; Raghavachari, K.; Trucks, G. W.; Pople, J. A. *J. Chem. Phys*. 1**991**, *94*, 7221.

(32) Frisch, M. J.; Trucks, G. W.; Schlegel, H. B.; Scuseria, G. E.; Robb, M. A.; Cheeseman, J. R.; Zakrzewsky, V. G.; Montgomery, J. A.; Stratman, R. E.; Burant, J. C.; Dapprich, S.; Millam, J. M.; Daniels, A. D.; Kudin, K. N.; Strain, M. C.; Farkas, O.; Tomasi, J.; Barone, V.; Cossi, M.; Gammi, R.; Mennucci, B.; Pomelli, C.; Adamo, C.; Clifford, S.; Ochterski, J.; Peterson, G. A.; Ayala, P. Y.; Cui, Q.; Morokuma, K.; Malick, D. K.; Rabuck, A. D.; Raghavachari, K.; Foresman, J. B.; Gioslowski, J.; Ortiz, J. V.; Stefanov, B. B.; Liu, G.; Liashenko, A.; Piskorz, P.; Komaromi, I.; Gomperts, R.; Martin, R. L.; Fox, D. J.; Keith, T.; Al-Laham, M. A.; Peng, C. Y.; Nanayakkara, A.; Gonzalez, C.; Challacombe, M.; Gill, P. M. W.; Johnson, B. G.; Chen, W.; Wong, M. W.; Andres, J. L.; Head-Gordon, M.; Replogle, E. S.; J. A. Pople, J. A. *Gaussian 98*, revision A.1; Gaussian, Inc.: Pittsburgh, PA, 1998.

(33) Robinson, P. J.; Holbrook, K. A. *Unimolecular Reactions*; Wiley-Interscience: New York, 1972.

(34) Steinfeld, J. I.; Francisco, J. S.; Hase, W. L. *Chemical Kinetics and Dynamics*; Prentice Hall: Englewood Cliffs, NJ, 1989.

(35) Gilbert, R. G.; Smith, S. C. *Theory of Unimolecular and Recombination Reactions*; Blackwell: London, 1990.

(36) Baer, T.; Hase, W. L. *Unimolecular Reaction Dynamics*; Oxford University Press: New York, 1996.

(37) Troe, J. *J. Chem. Phys*. **1977**, *66*, 4745.

(38) Gilbert, R. G.; Smith, S. C.; Jordan, M. J. T. *UNIMOL Program Suite*; Sydney University, NSW, 1993.